On the Computation of the Attenuation Constant by Using the Generalized Telegraphist's Equations Based Electromagnetic Analysis Method

Stefan Simion
Department of Electronics and Communications Engineering, MTA – Ferdinand I, 050141, Bucharest, Romania

Corresponding author: Stefan Simion (e-mail: stefan.simion@yahoo.com).

ABSTRACT Numerical results for the attenuation constant obtained by using the generalized telegraphist's equations (GTEs) based electromagnetic analysis method and comparison with the HFSS (High Frequency Structure Simulator) results are reported. To calculate the attenuation constant with the GTEs method, not only the amplitudes of the voltage modes but also the amplitudes of the current modes must be found. In this paper, new relations for the amplitudes of the current modes are proposed, which allow the accurate calculation of the attenuation constant. To validate these relations, the attenuation constants for homogeneous and different partially dielectric-filled rectangular waveguides are computed for the fundamental propagation mode by using the GTEs based analysis method and the results are compared with those obtained with HFSS. It is shown that using the revised relations for the amplitudes of the current modes, the GTE method can be used to compute accurately the propagation and attenuation constant, but only for propagation modes in which the components of the electric field are not oriented perpendicular to the interface between different dielectrics. This limitation is not due to the proposed current mode relations, but is due to the GTE method which cannot highlight the electric field discontinuities.

INDEX TERMS Attenuation constant, Generalized telegraphist's equations, Electromagnetic analysis method, Partially dielectric-filled rectangular waveguide.

I. INTRODUCTION

WAVEGUIDES are widely considered a viable solution for high microwave frequencies, due to their lower attenuation constants compared to transmission lines. Various numerical methods have been proposed for calculating the propagation parameters of the waveguide, mainly the propagation constant and the attenuation constant. For certain particular cross-section configurations of uniform metallic waveguides that are partially or completely filled with solid dielectrics, accurate analytical solutions to the electromagnetic problem are possible [1-6]. Also, different configurations of dielectric waveguides have been analyzed using approximate analytical methods [7] or semi analytical methods [8-10]. For waveguide configurations when analytical methods cannot be used to solve the electromagnetic field equations, numerical methods have been proposed. Reviews of these methods, as well as a comparison between them, are presented in [11,12] and [13], respectively. The best known numerical methods that can be used for the analysis of uniform waveguides of any shape and dielectric profile of the cross-section refer to the finite difference method [14-16], the finite element method [17-21] and methods that combine these two methods [22-24], but also the numerical method based on the generalized telegraphist's equations (GTE) [25-28]. Moreover, to reduce the computation time of cutoff frequencies of metallic waveguides, numerical techniques based on the meshless method [29,30] or the method of auxiliary sources with an excitation source [31,32] have been proposed and successfully applied.

Compared to the finite-difference/element methods, the GTE analysis method does not show spurious modes and moreover, the solutions for the propagation constant are stationary as a result of the Galerkin's procedure used to develop this numerical method.

The GTE based analysis method was used in [26] to calculate the propagation constants for different cross-section configurations of dielectric waveguides, as well as for determining the field configurations on different propagation modes, but no numerical results about the attenuation constant are provided. For this last task, the amplitudes of the current modes must also be computed. Note that only the amplitudes of the voltage modes are needed to calculate the propagation constant, but if the

values for the attenuation constants are required, the current modes must be known, too. Formulas for the current modes as a function of the voltage modes are given in [26], but they are not used to compute the attenuation constant. When used, it can be shown that huge differences for the attenuation constant compared to HFSS (High Frequency Structure Simulator) [33] are obtained for any cross-section waveguide configuration. New relations for the current mode amplitudes without any demonstration of them were first used in [34], where the attenuation constant for a dielectric waveguide was calculated with the GTE method and the results were compared with those obtained with HFSS. Small differences were observed between the values calculated by the two methods, but no analysis of these differences was performed for other waveguide configurations.

In this paper, the relations proposed in [34] for the current mode amplitudes are analytically demonstrated. Also, numerical results obtained with the GTE method are presented for the attenuation constants, as well as for the propagation constant, on the dominant modes that propagates on different rectangular metallic waveguides, homogeneously or partially filled with solid dielectrics. The results obtained with the GTE method are compared with those obtained with HFSS. It is shown that differences from the HFSS results can be observed for the propagation and attenuation constants, but not for all configurations of the analyzed cross-sections. Based on the representations of the transverse electric field obtained by GTE and HFSS analysis methods, it is explained why the results for the propagation and attenuation constants obtained with the GTE method could be different from those obtained with HFSS.

The paper is organized as follows. In Section II, although the GTE based analysis method has already been presented by other authors (see [25-28]), in order to improve the clarity of the whole paper, this method is also presented here briefly. However, unlike those already published, this section does not focus primarily on the theoretical aspects of the method, but on the formulas and details needed to implement this method. In Section III, the theoretical support for the relations between the voltage and current mode amplitudes proposed in this paper is presented. The formulas used for the calculation of the conductor and dielectric losses are given in Section IV. Section V is dedicated to numerical results that validate the proposed relations between voltage and current modes. The conclusions on the results obtained in this paper are presented at the end of the paper, in Section VI. In Appendix, the expressions of the functions mentioned in Section II are given.

II. DESCRIPTION OF THE ANALYSIS METHOD

If solid dielectrics are placed inside the hollow metallic waveguides, the propagation modes are different from the transverse magnetic (TM_{mn}) and transverse electric (TE_{mn}) modes which propagate through the hollow metallic waveguides. In this case, for any propagation mode, the expressions of the transverse electric and magnetic field components ($\mathbf{E}_t$ and $\mathbf{H}_t$, respectively) can be written as sums of contributions of the TM_{mn} and TE_{mn} propagations modes of the hollow metallic waveguide [25,26]. In the following, β is the propagation constant of the propagation mode having the field components $\mathbf{E}_t$ and $\mathbf{H}_t$.

In practice, a finite number of TE_{mn} and TM_{mn} modes of the hollow waveguide are taken into account. As much higher is the number of TM_{mn} and TE_{mn} modes taken into account, as much better is the numerical accuracy for $\mathbf{E}_t$ and $\mathbf{H}_t$. If $m_{\max}$ and $n_{\max}$ are the maximum values of the integer numbers m and n, respectively, for $R = m_{\max} = n_{\max}$, the number of TE_{mn} modes is $N = R^2 + 2R$, while the number of TM_{mn} modes is $M = R^2 < N$. In order to simplify the implementation of the GTE method, the TM_{mn} and TE_{mn} modes are combined in a single sum of N terms, assuming additional conditions for the TM_{mn} modes which are not allowed (i.e. TM_{mn} modes with $m = 0$ or $n = 0$ must not be taken into account).

Therefore, $\mathbf{E}_t$ and $\mathbf{H}_t$ can be written as [26]:

$$\mathbf{E}_t(x,y,z) = \exp(-\mathrm{j}\beta z)\cdot\sum_{i=1}^{N}\left[V_i^{TM}\mathbf{e}_i^{TM}(x,y) + V_i^{TE}\mathbf{e}_i^{TE}(x,y)\right] \tag{1a}$$

and

$$\mathbf{H}_t(x,y,z) = \exp(-\mathrm{j}\beta z)\cdot\sum_{i=1}^{N}\left[I_i^{TM}\mathbf{h}_i^{TM}(x,y) + I_i^{TE}\mathbf{h}_i^{TE}(x,y)\right] \tag{1b}$$

where $V_i^{TM/TE}$ and $I_i^{TM/TE}$ are the voltage and current mode amplitudes for the $i-$th TM_{mn}/TE_{mn} mode, respectively. Also, in (1a,b), $\mathbf{e}_i^{TM}(x,y) = -\nabla_t\Phi_i(x,y)$ and $\mathbf{h}_i^{TM}(x,y) = -\mathbf{z}_0\times\nabla_t\Phi_i(x,y)$, as well as $\mathbf{e}_i^{TE}(x,y) = \mathbf{z}_0\times\nabla_t\Psi_i(x,y)$ and $\mathbf{h}_i^{TE}(x,y) = -\nabla_t\Psi_i(x,y)$ are orthogonal functions of the $i-$th TM_{mn} and TE_{mn} propagation mode, respectively [1], $\nabla_t = \mathbf{x}_0\,\partial/\partial x + \mathbf{y}_0\,\partial/\partial y$ is the two-dimensional gradient operator, while $\mathbf{x}_0$, $\mathbf{y}_0$ and $\mathbf{z}_0$ are unit vectors in the x, y and z directions of the xyz coordinate system, respectively.

In this paper, the hollow metallic waveguide is considered rectangular, having the width a and the height b ($a > b$).

The functions Φ_i and Ψ_i are scalar functions of the $i-$th TM_{mn} and $i-$th TE_{mn} propagation mode, respectively, which are solutions of the Helmholtz equations, $(\nabla_t^2+k_{c,i}^2)\Phi_i(x,y)=0$ and $(\nabla_t^2+k_{c,i}^2)\Psi_i(x,y)=0$, where $k_{c,i}^2=(m_i\pi/a)^2+(n_i\pi/b)^2$ is the square of the cutoff wave number for the $i-$th mode, TM_{mn} and TE_{mn} as well, while m_i and n_i are the values of m and n, respectively, for this $i-$th mode ($i=1\ldots N$).

Solving the Helmholtz's equations for the scalar functions Φ_i and Ψ_i and imposing boundary conditions on the metallic walls of the rectangular hollow waveguide, the following expressions are obtained [1]:

$$\Phi_i(x,y)=\Phi_{0,i}\sin\left(\frac{m_i\pi}{a}x\right)\sin\left(\frac{n_i\pi}{b}y\right) \quad \text{and} \tag{2a}$$

$$\Psi_i(x,y)=\Psi_{0,i}\cos\left(\frac{m_i\pi}{a}x\right)\cos\left(\frac{n_i\pi}{b}y\right). \tag{2b}$$

In (2a), $\Phi_{0,i}=0$ for $m_i=0$ or $n_i=0$, while $\Phi_{0,i}=2/\pi(m_i^2b/a+n_i^2a/b)^{-1/2}$ for $n_i\neq 0$ and $m_i\neq 0$. In (2b), $\Psi_{0,i}=\Phi_{0,i}/K$, where $K=1$ for $n_i\neq 0$ and $m_i\neq 0$, while $K=\sqrt{2}$ for $m_i=0$ and $n_i\neq 0$, as well as for $m_i\neq 0$ and $n_i=0$. Also, $\Phi_{0,i}=\Psi_{0,i}=0$ for $m_i=n_i=0$.

Following the technique presented in [26], $2N$ coupled equations for the V_i^{TE} and V_i^{TM} voltage modes ($i=1\ldots N$) corresponding to the TE_{mn} and TM_{mn} propagation modes of the hollow waveguide can be obtained, for any mode that propagates along the dielectric-filled metallic waveguide. These coupled equations may be written in a matrix form, obtaining the characteristic eigenvalue equation $[M]\cdot[V]=\lambda\cdot[V]$, where $[M]$ is $2N\times 2N$ matrix, while λ and $[V]=[V_1^{TM}\ldots V_N^{TM}\ V_1^{TE}\ldots V_N^{TE}]^T$ are the eigenvalue and voltage eigenvector, respectively, for a particular propagation mode. The expressions for the elements of the matrix $[M]$ are given by:

$$M_{i,j}=\begin{cases}-k_0^2Y_1(i,j)+\sum_{k=1}^{N}Z_1(i,k)Y_1(k,j), \\ \quad \text{if } i=1\ldots N \text{ and } j=1\ldots N \\ -k_0^2Y_3(i-N,j), \\ \quad \text{if } i=(N+1)\ldots(2N) \text{ and } j=1\ldots N \\ -k_0^2Y_2(i,j-N)+\sum_{k=1}^{N}Z_1(i,k)Y_2(k,j-N), \\ \quad \text{if } i=1\ldots N \text{ and } j=(N+1)\ldots(2N) \\ -k_0^2Y_4(i-N,j-N)+\delta_{i-N,j-N}\cdot(k_{c,i-N})^2, \\ \quad \text{if } i=(N+1)\ldots(2N) \text{ and } j=(N+1)\ldots(2N)\end{cases} \tag{3}$$

where the functions Y_1, Y_2, Y_3, Y_4, and Z_1 are mentioned in the Appendix of this paper, while $\delta_{i,j}$ is Kronecker delta ($\delta_{i,j}=1$ if $i=j$ and $\delta_{i,j}=0$ if $i\neq j$).

Determining the eigenvalues of the matrix $[M]$, $2N$ solutions for λ are obtained, each belonging to a particular mode that propagates along the dielectric-filled metallic waveguide (N solutions for TE modes and N solutions for TM modes). A mode can propagate along the waveguide only if $\lambda<0$, when the propagation constant β is equal to $\sqrt{-\lambda}$. The higher the frequency of analysis, the more modes are allowed to propagate. The eigenvector $[V]$ is computed for each eigenvalue, λ.

III. RELATIONS BETWEEN THE VOLTAGE AND CURRENT MODE AMPLITUDES

If (1a,b) are used in the expressions given in Section II for $\mathbf{e}_i^{TM/TE}$ and $\mathbf{h}_i^{TM/TE}$, taking into account (2a,b), the electric and magnetic field components along the $x-$axis and $y-$axis may be written as $E_x=\sum_{i=1}^{N}E_{x,i}$, $E_y=\sum_{i=1}^{N}E_{y,i}$, $H_x=\sum_{i=1}^{N}H_{x,i}$ and $H_y=\sum_{i=1}^{N}H_{y,i}$ where:

$$E_{x,i}(x,y,z)=\exp(-j\beta z)\left(-V_i^{TM}\Phi_{0,i}\frac{m_i\pi}{a}+V_i^{TE}\Psi_{0,i}\frac{n_i\pi}{b}\right)\cdot\cos\left(\frac{m_i\pi}{a}x\right)\sin\left(\frac{n_i\pi}{b}y\right) \tag{4a}$$

$$E_{y,i}(x,y,z)=\exp(-j\beta z)\left(-V_i^{TM}\Phi_{0,i}\frac{n_i\pi}{b}-V_i^{TE}\Psi_{0,i}\frac{m_i\pi}{a}\right)\cdot\sin\left(\frac{m_i\pi}{a}x\right)\cos\left(\frac{n_i\pi}{b}y\right) \tag{4b}$$

$$H_{y,i}(x,y,z)=\exp(-\mathrm{j}\beta z)\left(-I_i^{TM}\Phi_{0,i}\frac{m_i\pi}{a}+I_i^{TE}\Psi_{0,i}\frac{n_i\pi}{b}\right)\cdot\cos\left(\frac{m_i\pi}{a}x\right)\sin\left(\frac{n_i\pi}{b}y\right) \tag{4c}$$

and

$$H_{x,i}(x,y,z)=\exp(-\mathrm{j}\beta z)\left(I_i^{TM}\Phi_{0,i}\frac{n_i\pi}{b}+I_i^{TE}\Psi_{0,i}\frac{m_i\pi}{a}\right)\cdot\sin\left(\frac{m_i\pi}{a}x\right)\cos\left(\frac{n_i\pi}{b}y\right) \tag{4d}$$

The longitudinal magnetic and electric field components can be obtained from the transverse field components, with the formulas [1]: $E_z=-\mathrm{j}(2\pi f\varepsilon_0)^{-1}\cdot[\partial H_y/\partial x-\partial H_x/\partial y]$ and $H_z=\mathrm{j}(2\pi f\mu_0)^{-1}\cdot[\partial E_y/\partial x-\partial E_x/\partial y]$, where f is the frequency. Using (4a-d), we can write $E_z=\sum_{i=1}^{N}E_{z,i}$ and $H_z=\sum_{i=1}^{N}H_{z,i}$, where:

$$E_{z,i}(x,y,z)=\frac{-\mathrm{j}}{2\pi f\varepsilon_0}\exp(-\mathrm{j}\beta z)I_i^{TM}\Phi_{0,i}k_{c,i}^2\cdot\sin\left(\frac{m_i\pi}{a}x\right)\sin\left(\frac{n_i\pi}{b}y\right) \tag{5a}$$

and

$$H_{z,i}(x,y,z)=\frac{-\mathrm{j}}{2\pi f\mu_0}\exp(-\mathrm{j}\beta z)V_i^{TE}\Psi_{0,i}k_{c,i}^2\cdot\cos\left(\frac{m_i\pi}{a}x\right)\cos\left(\frac{n_i\pi}{b}y\right) \tag{5b}$$

Each field component given by (4a-d) is a sum of TM_{mn} and TE_{mn} field components which may be written as follows:

$$E_{x,i}^{TM/TE}=E_{x,i}\big|_{V_i^{TE/TM}=0},\ E_{y,i}^{TM/TE}=E_{y,i}\big|_{V_i^{TE/TM}=0},$$

$$H_{x,i}^{TM/TE}=H_{x,i}\big|_{I_i^{TE/TM}=0}\ \text{and}\ H_{y,i}^{TM/TE}=H_{y,i}\big|_{I_i^{TE/TM}=0}.$$

On the other hand, these TM_{mn} and TE_{mn} field components are related to the longitudinal field components based on the following expressions [3]:

$$E_{x,i}^{TM}=-\mathrm{j}\beta/k_{c,i}^2\cdot\partial E_{z,i}/\partial x,\ E_{y,i}^{TM}=-\mathrm{j}\beta/k_{c,i}^2\cdot\partial E_{z,i}/\partial y,$$
$$H_{x,i}^{TM}=\mathrm{j}\omega\varepsilon_0/k_{c,i}^2\cdot\partial E_{z,i}/\partial y,$$
$$H_{y,i}^{TM}=-\mathrm{j}\omega\varepsilon_0/k_{c,i}^2\cdot\partial E_{z,i}/\partial x,$$
$$E_{x,i}^{TE}=-\mathrm{j}\omega\mu_0/k_{c,i}^2\cdot\partial H_{z,i}/\partial y,$$
$$E_{y,i}^{TE}=\mathrm{j}\omega\mu_0/k_{c,i}^2\cdot\partial H_{z,i}/\partial x,$$

$$H_{x,i}^{TE}=-\mathrm{j}\beta/k_{c,i}^2\cdot\partial H_{z,i}/\partial x\ \text{and}\ H_{y,i}^{TE}=-\mathrm{j}\beta/k_{c,i}^2\cdot\partial H_{z,i}/\partial y.$$

Using (4a-d) and (5a,b) in the latter expressions, eight conditions are obtained which are satisfied for any i from 1 to N, only if:

$$V_i^{TM}/I_i^{TM}=\beta/(2\pi f\varepsilon_0)\ \text{and} \tag{6a}$$

$$V_i^{TE}/I_i^{TE}=2\pi f\mu_0/\beta. \tag{6b}$$

Formulas (6a,b) are different from those proposed in [26], where instead of using the propagation constant β of the mode consisting of superposition of TM_{mn} and TE_{mn} modes, the propagation constant $\beta_i=(k_0^2-k_{c,i}^2)^{1/2}$ is used for the $i-$th TM_{mn} or TE_{mn} mode, where $k_0=\omega/c_0$ is the free space wave number and c_0 is the speed of light.

Knowing the voltage and current eigenvectors, the field components can be computed using the expressions given in Section III. Then, the attenuation constants due to the conductor and dielectric losses can be computed as presented in the next section. However, the GTE method cannot model the field discontinuities between different dielectrics [26]. Therefore, as shown in Section V, the attenuation constant values computed with the GTE method for certain propagation modes could be wrong.

IV. CONDUCTOR AND DIELECTRIC LOSSES

The attenuation constants due to the conductor and dielectric losses for a certain mode that propagates through the waveguide are given by the general formulas $\alpha_c=(1/2)\cdot P_c/P$ and $\alpha_d=(1/2)\cdot P_d/P$, respectively, where:

$$P=\frac{1}{2}\cdot\mathrm{Re}\left\{\sum_{i=1}^{N}\left[V_i^{TM}\cdot\left(I_i^{TM}\right)^*+V_i^{TE}\cdot\left(I_i^{TE}\right)^*\right]\right\} \tag{7a}$$

is the power flowing down the waveguide,

$$P_c=\frac{R_s}{2}\cdot\left[\int_0^a C_1(x)\mathrm{d}x+\int_0^b C_2(y)\mathrm{d}y\right] \tag{7b}$$

is the power loss in the metallic walls,

$$P_d=\pi f\varepsilon_0\cdot\sum_{k=1}^{L}\left[\varepsilon_{r,k}\cdot\tan\delta_{\varepsilon_{r,k}}\cdot\iint_{S_{\varepsilon_{r,k}}}C_3(x,y)\mathrm{d}x\mathrm{d}y\right] \tag{7c}$$

is the power loss in the solid dielectrics inside the waveguide, while $R_s=(\pi f\mu_0/\sigma_\mathrm{m})^{1/2}$ is the surface resistance of the metallic walls of conductivity σ_m, L is

the number of different values of the dielectric constants $\varepsilon_{r,k}$ ($k=1...L$) and $S_{\varepsilon_{r,k}}$ is the cross-section area occupied by the solid dielectric of dielectric constant $\varepsilon_{r,k}$ and loss tangent $\tan\delta_{\varepsilon_{r,k}}$.

Also, in (7b,c):

$$C_1(x)=$$
$$|H_x(x,0,z)|^2+|H_z(x,0,z)|^2+|H_x(x,b,z)|^2+|H_z(x,b,z)|^2,$$

$$C_2(y)=$$
$$|H_y(a,y,z)|^2+|H_z(a,y,z)|^2+|H_y(0,y,z)|^2+|H_z(0,y,z)|^2$$

and

$$C_3(x,y)=|E_x(x,y,z)|^2+|E_y(x,y,z)|^2+|E_z(x,y,z)|^2,$$

where (4a-d) and (5a, b) must be taken into account to obtain the numerical values of these functions.

V. NUMERICAL RESULTS

Following the method presented in the previous sections, the propagation and attenuation constants on the fundamental mode were calculated for three waveguide cross-section configurations, all involving rectangular metallic waveguides. The first case concerns the homogeneous dielectric-filled rectangular waveguide (HDFRW), while the other two refer to partially dielectric filled rectangular waveguides (PDFRW-1 and PDFRW-2) with the cross sections shown in Fig. 1. All three waveguides are homogeneous along the propagation $z-$ axis.

The GTE based method presented in Sections II and III, as well as the formulas given in Section IV for the attenuation constants due to the conductor and dielectric losses have been implemented in MATHCAD [35].

For the numerical results presented in the following, the conductivity of the waveguide metallic walls is equal to $5.8\cdot10^7$ S/m (copper).

A. HDFRW ANALYSIS

A WR90 rectangular metallic waveguide ($a=22.86$ mm and $b=10.16$ mm) is filled with homogeneous dielectric having $\varepsilon_r=2.25$ and $\tan\delta_{\varepsilon_r}=0.001$. For this particular case, trans-verse electric and magnetic modes propagate through the waveguide and the fundamental mode is TE_{10}. This waveguide was analysed for the propagation and attenuation constants of the fundamental mode, by using the GTE method and HFSS. The results are plotted in Fig. 2, where no differences have been observed between values obtained by the two analysis methods. Also, the numerical values for the propagation and attenuation constants are the same with those obtained by the closed formulas (see for example [3]). This perfect match can be explained as follows.

If the dielectric fills homogeneously the entire cross section of the waveguide, from Appendix, $Y_1(i,j)$ and $Y_4(i,j)$ are equal to ε_r if $i=j$ and equal to 0 if $i\neq j$, while $Y_2(i,j)$ and $Y_3(i,j)$ are equal to 0, for any i and j.

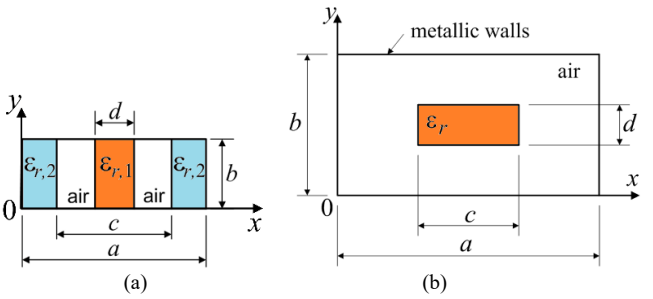

FIGURE 1. Cross-section configurations for the partially dielectric-filled rectangular waveguides analyzed in this paper: PDFRW-1 (a) and PDFRW-2 (b).

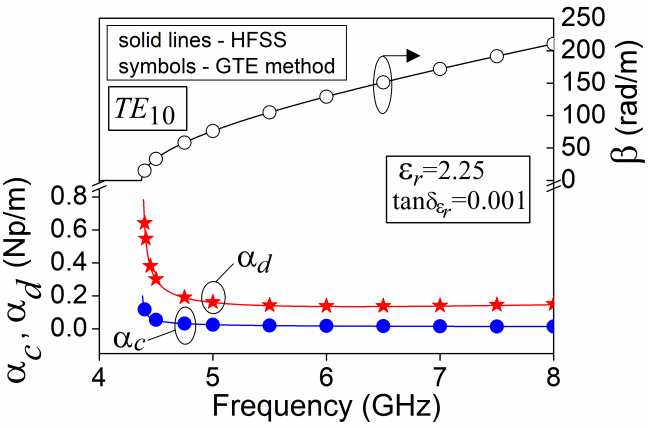

FIGURE 2. Numerical results for the propagation and attenuation constants obtained with the GTE based method and with HFSS, for HDFRW on the TE_{10} mode,

Also, $Z_1(i,j)$ is equal to k_0^2/ε_r if $i=j$ and equal to 0 if $i\neq j$. Therefore, $M_{i,j}$ given by (3) are equal to 0 if $i\neq j$, so that $[M]$ is a diagonal matrix. In this case, for a particular mode that propagates along the waveguide, only one element of the eigenvector $[V]=[V_1^{TM}...V_N^{TM}\ V_1^{TE}...V_N^{TE}]^T$ is different from zero. If the mode under analysis is TE_{10}, the voltage mode different from zero is V_i^{TE}, where i is the index number corresponding to the TE_{10} mode that propagates along the empty metallic waveguide. When the dielectric fills the entire cross section, the same results for the propagation and attenuation constants are obtained for small value of R, as well as for high values of R. In this case, the minimum

value of R must be chosen such as the propagation mode under analysis to be taken into account.

For any mode propagates along the metallic waveguide filled homogeneously with dielectric, it can be shown that the expressions for the electric and magnetic field components given by (4a-d) and (5a,b) may be reduced to the well-known forms published in many microwave books (see for example [1-3]). For this reason, there is no difference between the values of the propagation and attenuation constants obtained with GTE method and the values obtained using closed formulas [3].

B. PDFRW-1 ANALYSIS

A WR90 rectangular metallic waveguide partially filled with solid dielectrics as shown in Fig. 1a has been analysed with the GTEs based analysis method and with the HFSS software. The following input geometric data were imposed: $a = 22.86$ mm, $b = 10.16$ mm, $c = 16$ mm and $d = 8$ mm.

Two cases have been analysed for the fundamental TE_{10} propagation mode. The first case corresponds to the situation when the dielectrics are the same, $\varepsilon_{r,1} = \varepsilon_{r,2} = 4.4$ and also $\tan\delta_{\varepsilon_{r,1}} = \tan\delta_{\varepsilon_{r,2}} = 0.02$. The second case corresponds to the situation when two different solid dielectrics partially fill the waveguide: $\varepsilon_{r,1} = 2.25$, $\varepsilon_{r,2} = 4.4$, $\tan\delta_{\varepsilon_{r,1}} = 0.001$ and $\tan\delta_{\varepsilon_{r,2}} = 0.02$.

Numerical results for the propagation constant, as well as for the attenuation constants due to the conductor and dielectric losses are presented in Fig. 3, for R = 5 (35 TE modes and 25 TM modes have been taken into account).

For different values of R, the normalized propagation constant and attenuation constants computed with the GTE method at 6.5 GHz are given in Table I. As it is observed, the changes in the values of these parameters are small, if R is greater than 5.

The TE_{10} transverse and longitudinal electric field magnitudes for the case of two different solid dielectrics have been also obtained with the GTE based analysis method and with HFSS, at 6.5 GHz (the waveguide length is equal to 50 mm). The results are presented in Fig. 4.

From Figs. 3 and 4, very good agreement between the results obtained with the GTE based analysis method and HFSS is observed for PDFRW-1. For this propagation mode, there is no discontinuity in the electric field. For this reason, the electric field representations obtained with the GTE method are in very good agreement with those obtained with HFSS, as well as the propagation and attenuation constant values obtained by the two methods of analysis.

Since the conductor and dielectric losses, as well as the transverse electric field configuration depend on the amplitudes of the current modes, the good agreement between the results obtained with the GTE method and with HFSS validates the relations between the amplitudes of the voltage and current modes proposed in this paper.

TABLE I. Normalized Propagation Constant and Attenuation Constants Computed for PDFRW-1, for Different Values of R, at 6.5 GHz.

R	β/β_0	α_c (Np/m)	α_d (Np/m)
3	0.861	0.018	0.377
4	0.862	0.018	0.356
5	0.863	0.018	0.356
6	0.868	0.019	0.365
7	0.868	0.019	0.365

C. PDFRW-2 ANALYSIS

For the second dielectric-filled waveguide configuration, the following input data have been assumed: $c = 5.7$ mm, $d = 2.8$ mm and $a = 2b = 25$ mm, while $\varepsilon_r = 2.4$ and the dielectric rod tangent loss is equal to 0.0055 (see Fig. 1b).

This waveguide was also analyzed in [30] for the first four propagation modes, where the main purpose was the study of the mode matching between the dielectric waveguide and the rectangular hollow metallic waveguide, as well as the simulation conditions of the dielectric waveguide in relation to the size of the metallic waveguide.

Using the GTE based numerical method presented in Section II, the propagation constant β for the E_{11}^{y} fundamental mode was computed at different frequencies, for R = 7 (63 TE modes and 49 TM modes have been taken into account) and R = 9 (99 TE modes and 81 TM modes have been taken into account).

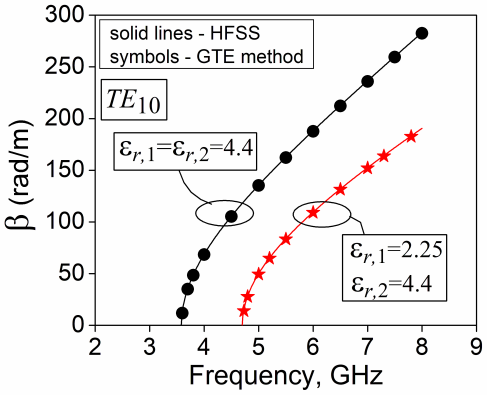

(a)

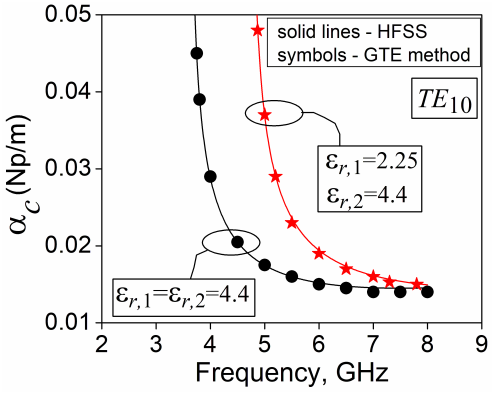

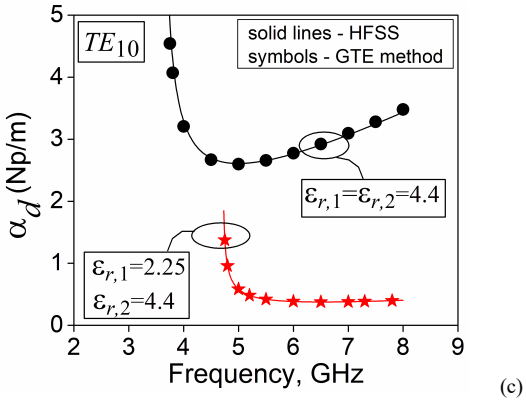

FIGURE 3. Numerical results obtained with the GTE based method (R=5) and with HFSS on the TE_{10} mode, for PDFRW-1 (see Fig. 1a): the propagation constant (a), the attenuation constant due to the losses in the metallic walls (b) and the attenuation constant due to the losses in the solid dielectric (c).

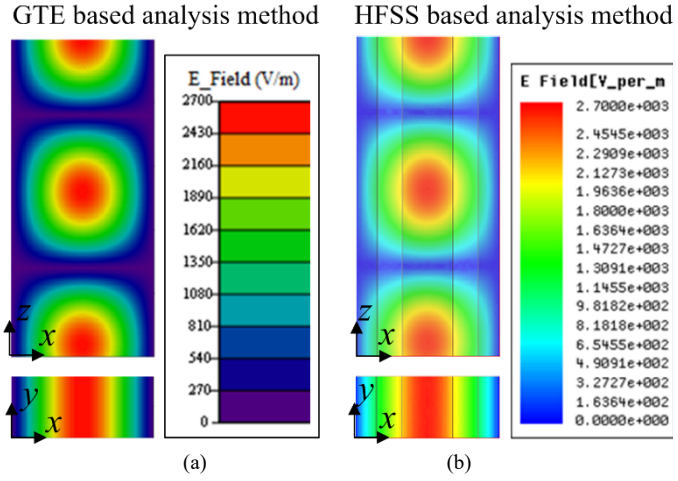

FIGURE 4. TE_{10} transverse and longitudinal electric field magnitudes obtained at 6.5 GHz for PDFRW-1 (see Fig. 1a) with the GTE based analysis method for R=5 (a) and with HFSS (b).

The results for the propagation constant have been normalized to the free space wave number k_0, and this ratio is presented graphically in Fig. 5, where, for comparison, the results obtained with HFSS have been also plotted. The graph shows that increasing the number of modes taking into account in the GTE based analysis method (i.e. increasing the value of R), the results are getting closer to the HFSS results.

The attenuation constants α_c and α_d due to the losses in the metallic walls and the dielectric rectangular rod, respectively, were also computed using the GTE method and the results were compared with HFSS. The numerical values obtained for α_d / α_c showed that this ratio increases rapidly as the frequency increases, going toward 10^4 for frequencies around 50GHz. Therefore, the overall attenuation constant $\alpha = \alpha_c + \alpha_d$ approaches α_d.

The variation of the attenuation constant α versus the

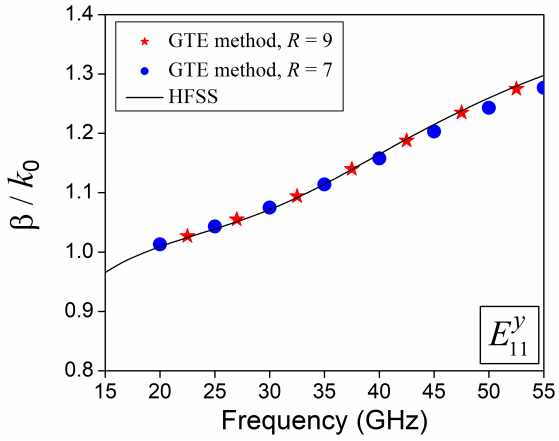

FIGURE 5. Normalized propagation constant versus the frequency, obtained with the GTE analysis method and with HFSS, for the E_{11}^y mode propagates on PDFRW-2 (see Fig. 1b).

frequency is shown in Fig. 6, where the results obtained by using the GTE numerical method are represented by symbols, while the HFSS results are given by solid line. It is observed that the results obtained with the GTE method for R equal to 7 are practically the same as for R equal to 9. Therefore, the difference from the HFSS results is not due to the fact that the value of R is too small, but, as shown below, is due to the discontinuities of the transverse electric field observed in the HFSS results and which cannot be highlighted by the GTE method. From Fig. 6, the GTE method overestimates the attenuation constant compared to the values obtained with HFSS.

The differences between the values obtained with the GTE method for R at the same frequency are small, so that, for clarity, the symbols for different R values were plotted intercalated in Figs. 5 and 6.

The normalized propagation constant and attenuation constants computed with the GTE method at 40 GHz for different values of R are given in Table II. Small changes in the values of these parameters are observed for R greater than 9.

The magnitude of the transverse electric field for the E_{11}^y mode is presented in Fig. 7, for R = 9, at 40 GHz. Compared to HFSS results, no discontinuities in the field

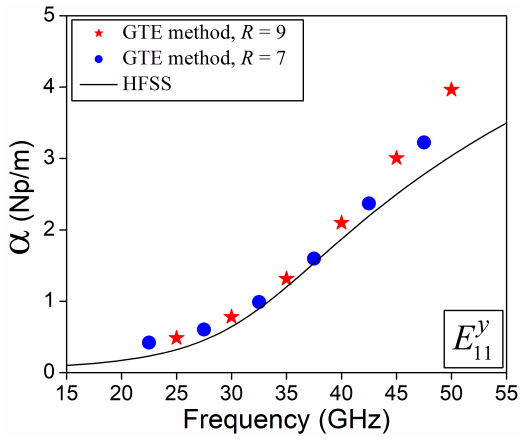

FIGURE 6. The overall attenuation constant versus the frequency, obtained with the GTE analysis method and with HFSS, for the E_{11}^y mode propagates on PDFRW-2 (see Fig. 1b).

TABLE II. Normalized Propagation Constant and Attenuation Constants Computed for PDFRW-2, for Different Values of *R*, at 40 GHz.

R	β/β_0	α_c (Np/m)	α_d (Np/m)
5	1.131	0.002452	1.548
6	1.152	0.00203	1.866
7	1.152	0.0028	1.851
8	1.158	0.002609	1.967
9	1.165	0.002531	2.075
10	1.166	0.002505	2.083

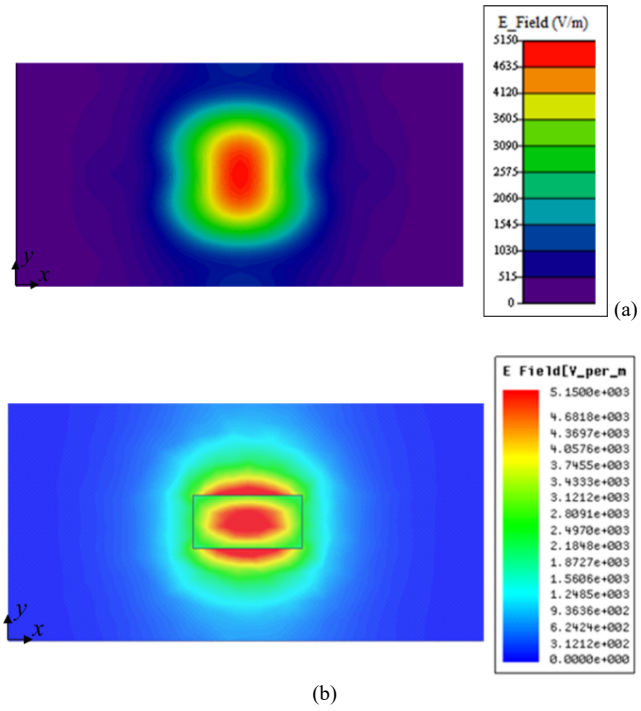

FIGURE 7. Magnitudes of the transverse electric field for the E_{11}^y mode that propagates on PDFRW-2 (see Fig. 1b) at 40 GHz, obtained with the GTE analysis method when *R*=9 (a) and with HFSS (b).

representation at the interface between the dielectric rod and air are observed in the results obtained with the GTE method. The difference between the representations of the transverse electric field obtained by the two methods may explain why the differences between the values of the attenuation constants obtained by the GTE and HFSS method are not small.

From Fig. 8, because $E_y >> E_x$ for E_{11}^y, no difference can be seen between the results obtained with the GTE method and HFSS for the longitudinal electric field magnitude on the E_{11}^y mode ($y = b/2$ and the waveguide length is equal to 20 mm). This may explain why the results for the propagation constant obtained with the GTE and HFSS methods are practically the same, if the value of *R* is high enough (see Fig. 5).

VI. CONCLUSION

New relations for the amplitudes of the current modes used in the GTEs based analysis method have been proposed. The correctness of these formulas is a condition to obtain correct values of the attenuation constant by using the GTE based numerical method. To validate the proposed relations, homogeneous dielectric-filled rectangular metallic waveguide and two partially dielectric-filled rectangular

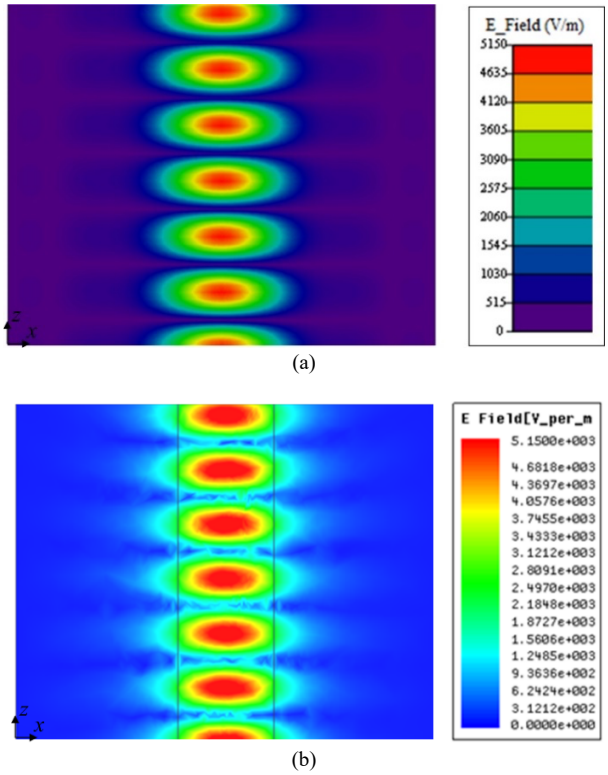

FIGURE 8. Magnitudes of the electric field along the PDFRW-2 (see Fig. 1b) for the E_{11}^y mode at 40 GHz and *y* = *b*/2, obtained with the GTE analysis method when *R*=9 (a) and with HFSS (b).

metallic waveguides have been analyzed for the propagation and attenuation constants, as well as for the transverse and longitudinal electric field distributions, on the fundamental propagation modes. The results obtained with the GTE method were compared with those obtained with HFSS, and the following conclusions can be drawn:

- For the homogeneous dielectric-filled waveguide, the results obtained with the GTE method match the HFSS results perfectly for the propagation constant, as well as for the attenuation constants.
- For the first partially dielectric-filled rectangular metallic waveguide (PDFRW-1, see Fig. 1a), there is no discontinuity of the electric field on the TE_{10} fundamental propagation mode, and the transverse and longitudinal electric field obtained with the GTE method and HFSS are the same (see Fig. 4). For this reason, the results obtained with the GTE method for the propagation and attenuation constants converge to those obtained with HFSS.
- For the second partially dielectric-filled rectangular metallic waveguide (PDFRW-2, see Fig. 1b), the transverse electric field obtained with HFSS for the propagation mode E_{11}^{y} shows discontinuities at the interface between the solid dielectric and air which cannot be highlighted by the GTE analysis method. As a result, the values for the attenuation constant obtained with the GTE method are different from those obtained with HFSS (see Fig. 6).
- Electric field discontinuities are present only for propagation modes with electric field components that are oriented perpendicular to the interface between different dielectrics. This is the situation for PDFRW-2, but not for PDFRW-1. Because the GTE method cannot highlights these electric field discontinuities, the electric field obtained by using this method is not accurate for PDFRW-2, but it is accurate for PDFRW-1. For this reason, the attenuation constant obtained with the GTE method converge to the values obtained with HFSS for PDFRW-1, but not for PDFRW-2 (see Fig. 3 compared to Fig. 6).

The formulas proposed in this paper for the amplitudes of the current modes can be used to compute accurately the attenuation constants of partially dielectric-filled waveguides, for the propagation modes in which the components of the electric field are not oriented perpendicular to the interface between different dielectrics. These propagation modes include the TE_{10} fundamental mode which are allowed on the partially dielectric-filled waveguides with $y-$axis dielectric homogeneity.

Despite the computation time which is longer compared to HFSS, the GTE analysis method can be useful for calculating the field components for a propagation mode, but also as an alternative solution to the results obtained with a commercial analysis software.

APPENDIX

In this Appendix, L is the number of different values of the dielectric constants $\varepsilon_{r,k}$ $(k=1...L)$ and $S_{\varepsilon_{r,k}}$ is the cross-section area occupied by the solid dielectric of dielectric constant $\varepsilon_{r,k}$.

The functions used in (3) have the following expressions:

$$Y_1(i,j)=\begin{cases}0, & \text{if } n_t=0 \text{ or } m_t=0, \text{ where } t=i \text{ or } j\\ \delta_{i,j}+\sum_{k=1}^{L}(\varepsilon_{r,k}-1)F_{11}(i,j,S_{\varepsilon_{r,k}}), & \\ & \text{if } n_t\neq 0 \text{ and } m_t\neq 0, \text{ where } t=i \text{ or } j\end{cases},$$

$$Y_2(i,j)=\begin{cases}0, & \text{if } n_i=0 \text{ or } m_i=0\\ \sum_{k=1}^{L}(\varepsilon_{r,k}-1)F_{21}(i,j,S_{\varepsilon_{r,k}}), & \text{if } n_i\neq 0 \text{ and } m_i\neq 0\end{cases},$$

$$Y_3(i,j)=\begin{cases}0, & \text{if } n_j=0 \text{ or } m_j=0\\ \sum_{k=1}^{L}(\varepsilon_{r,k}-1)F_{31}(i,j,S_{\varepsilon_{r,k}}), & \text{if } n_j\neq 0 \text{ and } m_j\neq 0\end{cases},$$

$$Y_4(i,j)=\delta_{i,j}+\sum_{k=1}^{L}(\varepsilon_{r,k}-1)\cdot F_{41}(i,j,S_{\varepsilon_{r,k}})$$

and

$$Z_1(i,j)=\begin{cases}0, & \text{if } n_t=0 \text{ or } m_t=0, \text{ where } t=i \text{ or } j\\ \left(k_{c,i}k_{c,j}\right)^2\left[\delta_{i,j}\left(k_{c,i}\right)^{-2}-\sum_{k=1}^{L}\frac{\varepsilon_{r,k}-1}{\varepsilon_{r,k}}F_{51}(i,j,S_{\varepsilon_{r,k}})\right] & \\ & \text{if } n_t\neq 0 \text{ and } m_t\neq 0, \text{ where } t=i \text{ or } j\end{cases}$$

where

$$F_{11}(i,j,S_{\varepsilon_{r,k}})=\Phi_{0,i}\Phi_{0,j}\pi^2\cdot\left[\frac{n_i\cdot n_j}{b^2}\cdot I_1(i,j,S_{\varepsilon_{r,k}})+\frac{m_i\cdot m_j}{a^2}\cdot I_2(i,j,S_{\varepsilon_{r,k}})\right],$$

$$F_{21}(i,j,S_{\varepsilon_{r,k}})=\Phi_{0,i}\Psi_{0,j}\pi^2\cdot\left[\frac{n_i\cdot m_j}{ab}\cdot I_1(i,j,S_{\varepsilon_{r,k}})-\frac{m_i\cdot n_j}{ab}\cdot I_2(i,j,S_{\varepsilon_{r,k}})\right],$$

$$F_{31}(i,j,S_{\varepsilon_{r,k}})=\Phi_{0,j}\Psi_{0,i}\pi^2\cdot\left[\frac{m_i\cdot n_j}{ab}\cdot I_1(i,j,S_{\varepsilon_{r,k}})-\frac{n_i\cdot m_j}{ab}\cdot I_2(i,j,S_{\varepsilon_{r,k}})\right],$$

$$F_{41}(i,j,S_{\varepsilon_{r,k}})=\Psi_{0,i}\Psi_{0,j}\pi^2\cdot\left[\frac{m_i\cdot m_j}{a^2}\cdot I_1(i,j,S_{\varepsilon_{r,k}})+\frac{n_i\cdot n_j}{b^2}\cdot I_2(i,j,S_{\varepsilon_{r,k}})\right]$$

and

$$F_{51}(i,j,S_{\varepsilon_{r,k}}) = \Phi_{0,i} \cdot \Phi_{0,j} \cdot I_3(i,j,S_{\varepsilon_{r,k}}).$$

Also,

$$I_1(i,j,S_{\varepsilon_{r,k}}) = \iint\limits_{S_{\varepsilon_{r,k}}} \sin\left(\frac{m_i\pi}{a}x\right)\sin\left(\frac{m_j\pi}{a}x\right)\cos\left(\frac{n_i\pi}{b}y\right)\cos\left(\frac{n_j\pi}{b}y\right)\mathrm{d}x\mathrm{d}y,$$

$$I_2(i,j,S_{\varepsilon_{r,k}}) = \iint\limits_{S_{\varepsilon_{r,k}}} \cos\left(\frac{m_i\pi}{a}x\right)\cos\left(\frac{m_j\pi}{a}x\right)\sin\left(\frac{n_i\pi}{b}y\right)\sin\left(\frac{n_j\pi}{b}y\right)\mathrm{d}x\mathrm{d}y$$

and

$$I_3(i,j,S_{\varepsilon_{r,k}}) = \iint\limits_{S_{\varepsilon_{r,k}}} \sin\left(\frac{m_i\pi}{a}x\right)\sin\left(\frac{m_j\pi}{a}x\right)\sin\left(\frac{n_i\pi}{b}y\right)\sin\left(\frac{n_j\pi}{b}y\right)\mathrm{d}x\mathrm{d}y.$$

where the expressions of $\Phi_{0,i}$ and $\Psi_{0,i}$ have been given in Section II, as well as the expression of the cutoff wave number, $k_{c,i}$.

REFERENCES

[1] N. Marcuvitz, "Waveguide handbook", vol. 10 of the *MIT Radiation Laboratory Series*, McGraw Hill, 1951.

[2] R. E. Collin, "Foundations for microwave engineering – second edition", John Wiley & Sons, 2001.

[3] D. M. Pozar, "Microwave Engineering – fourth edition", John Wiley & Sons, 2012.

[4] L. Jin, R. M. A. Lee, and I. Robertson, "Analysis and design of a novel low-loss hollow substrate integrated waveguide", *IEEE Trans. Microw. Theory Tech.*, vol. 62, no. 8, pp. 1616–1624, August 2014, doi: 10.1109/TMTT.2014.2328555.

[5] P. H. Vartanian, W. P. Ayres, and A. L. Helgesson, "Propagation in dielectric slab loaded rectangular waveguide", *IRE Trans. Microw. Theory Tech.*, vol. 6, no. 2, pp. 215–222, Feb. 1958, doi: 10.1109/TMTT.1958.1124541.

[6] S. Simion, "Partially dielectric-filled rectangular waveguide configuration, proposed for broadband and low loss substrate integrated waveguides design", *Prog. Electromagn. Res. M*, vol. 94, pp. 73–82, 2020, doi: 10.2528/PIERM20051302.

[7] E. A. J. Marcatili, "Dielectric rectangular waveguide and directional coupler for integrated optics", *Bell Syst. Techn. J.*, vol. 48, no. 7, pp. 2071–2102, Sept. 1969, doi: 10.1002/j.1538-7305.1969.tb01166.x.

[8] K. Solbach, I. Wolff, "The electromagnetic fields and the phase constants of dielectric image lines", *IEEE Trans. Microw. Theory Tech.*, vol. 26, no. 4, pp. 266–274, April 1978, doi: 10.1109/TMTT.1978.1129363.

[9] R. Mittra, Y. L. Hou, V. Jamnejad, "Analysis of open dielectric waveguides using mode-matching technique and variational methods", *IEEE Trans. Microw. Theory Tech.*, vol. 28, no. 1, pp. 36–43, Jan. 1980, doi: 10.1109/TMTT.1980.1130003.

[10] C. G. Wells, J. A. R. Ball, "Mode-matching analysis of a shielded rectangular dielectric-rod waveguide", *IEEE Trans. Microw. Theory Tech.*, vol. 53, no. 10, pp. 3169–3177, Oct. 2005, doi: 10.1109/TMTT.2005.855148.

[11] J. B. Davies, "Review of methods for numerical solution of hollow-waveguide problem", *Proc. Inst. Electr. Eng.*, vol. 119, no. 1, pp. 33–37, Jan. 1972, doi: 10.1049/piee.1972.0004.

[12] S. M. Saad, "Review of numerical methods for the analysis of arbitrarily-shaped microwave and optical dielectric waveguides", *IEEE Trans. Microw. Theory Tech.*, vol. 33, no. 10, pp. 894–899, Oct. 1985, doi: 10.1109/TMTT.1985.1133147.

[13] F. L. Ng, "Tabulation of methods for the numerical solution of the hollow waveguide problem", *IEEE Trans. Microw. Theory Tech.*, vol. 22, no. 3, pp. 322–329, March 1974, doi: 10.1109/TMTT.1974.1128217.

[14] D. G. Corr, J. B. Davies, "Computer analysis of the fundamental and higher order modes in single and coupled microstrip", *IEEE Trans. Microw. Theory Tech.*, vol. 20, no. 10, pp. 669–678, Oct. 1972, doi: 10.1109/TMTT.1972.1127842.

[15] E. Schweig, W. B. Bridges, "Computer analysis of dielectric waveguides: a finite difference method", *IEEE Trans. Microw. Theory Tech.*, vol. 32, no. 5, pp. 531–541, May 1984, doi: 10.1109/TMTT.1984.1132717.

[16] K. Bierwirth, N. Schulz, F. Arndt, "Finite-difference analysis of rectangular dielectric waveguide structures", *IEEE Trans. Microw. Theory Tech.*, vol. 34, no. 11, pp. 1104–1114, Nov. 1986, doi: 10.1109/TMTT.1986.1133506.

[17] S. Ahmed, P. Daly, "Finite-element methods for inhomogeneous waveguides", *Proc. Inst. Electr. Eng.*, vol. 116, no. 10, pp. 1661–1664, Oct. 1969, doi: 10.1049/piee.1969.0300.

[18] C. Yeh, S. B. Dong, W. Oliver, "Arbitrarily shaped inhomogeneous optical fiber or integrated optical waveguides", *J. Appl. Phys.*, vol. 46, pp. 2125–2129, Nov. 1975, doi: 10.1063/1.321851.

[19] C. Yeh, K. Ha, S. B. Dong, W. P. Brown, "Single mode optical waveguides", *Applied Optics*, vol. 18, no. 10, pp. 1490–1504, Nov. 1979, doi: 10.1364/AO.18.001490.

[20] N. Mabaya, P. E. Lagasse, P. Vandenbulcke, "Finite element analysis of optical waveguides", *IEEE Trans. Microw. Theory Tech.*, vol. 29, no. 6, pp. 600–605, June 1981, doi: 10.1109/TMTT.1981.1130400.

[21] K. S. Chiang, "Finite element method for cutoff frequencies of weakly guiding fibers of arbitrary cross-section", *Opt. Quantum Electron.*, vol. 16, no. 6, pp. 487–493, Nov. 1984, doi: 10.1007/BF00619910.

[22] B. Zhu, J. Chen, W. Zhong, "A hybrid finite-element / finite-difference method with implicit-explicit time stepping scheme for Maxwell's equations", *IEEE Int. Conf. on Microwave Technology & Computational Electromagnetics*, Beijing, China, May 2011, doi: 10.1109/ ICMTCE.2011.5915564.

[23] D. Koh, H. Lee, T. Itoh, "A hybrid full-wave analysis of via-hole grounds using finite-difference and finite element time-domain methods", *IEEE Trans. Microw. Theory Tech.*, vol. 45, no. 12, pp. 2217–2223, Dec. 1997, doi: 10.1109/22.643819.

[24] M. Yang, Y. Chen, R. Mittra, "Hybrid finite-difference/finite-volume time-domain analysis for microwave integrated circuits with curved PEC surfaces using nonuniform rectangular grid", *IEEE Trans. Microw. Theory Tech.*, vol. 48, no. 6, pp. 969–975, June 2000, doi: 10.1109/ 22.846728.

[25] S.A. Schelkunoff, "Generalized telegraphist's equations for waveguides", *Bell Syst. Tech. J.*, vol. 31, no. 4, pp. 784–801, July 1952, doi: 10.1002/j.1538-7305.1952.tb01406.x.

[26] K. Ogusu, "Numerical analysis of the rectangular dielectric waveguide and its modifications", *IEEE Trans. Microw. Theory Tech.*, vol. 25, no. 11, pp. 874–885, Nov. 1977, doi: 10.1109/TMTT.1977.1129235.

[27] L.C.L. So, C.A. Lee, "Verification of generalized telegraphist's equations applied to dielectric waveguide problems", *Appl. Opt.*, vol. 31, no. 30, pp. 6446–6452, Oct. 1992, doi: 10.1364/AO.31.006446.

[28] L. Weiss, W. Mathis, "Generalized telegraphist's equations for deformed waveguides", *Electromagnetics*, vol. 18, no. 4, pp. 353–365, 1998, doi: 10.1080/02726349808908594.

[29] V. Lombardi, M. Bozzi, L. Perregrini, "An improved meshless method for waveguide eigenvalue problems", *IEEE Microw. Wirel. Compon. Lett.*, vol. 27, no. 12, pp. 1047–1049, Dec. 2017, doi: 10.1109/LMWC.2017.2751302.

[30] V. Lombardi, M. Bozzi, L. Perregrini, "A novel variational meshless method with radial basis functions for waveguide eigenvalue problems", *IEEE Trans. Microw. Theory Tech.*, vol. 66, no. 8, pp. 3714–3723, Aug. 2018, doi: 10.1109/TMTT.2018.2830765.

[31] M. Kouroublakis, N. L. Tsitsas, G. Fikioris "Mode analysis by the method of auxiliary sources with an excitation source", *IEEE Trans. Microw. Theory Tech.*, vol. 69, no. 6, pp. 2960–2971, June 2021, doi: 10.1109/TMTT.2021.3073400.
[32] M. Kouroublakis, N. L. Tsitsas, G. Fikioris "Method of auxiliary sources with an excitation source: The auxiliary-current vector norm", *IEEE Microw. Wirel. Compon. Lett.*, vol. 32, no. 5, pp. 371–374, May 2022, doi: 10.1109/LMWC.2021.3137021.
[33] *High Frequency Structure Simulator (HFSS) – User's guide* (Ansoft Corporation).
[34] S. Simion, "On the analysis of the rectangular dielectric waveguide, by using the generalized telegraphist's equations based method", in *Proc. IEEE Int. Semic. Conf.*, Sinaia, Romania, Oct. 6–8, 2021, pp. 45–48, doi: 10.1109/CAS52836.2021.9604181.
[35] *Mathcad – User's guide* (MathSoft, Inc.).